On the Stability of Circular Orbits of Particles Moving around Black Holes Surrounded by Axially Symmetric Structures

Patricio.S. Letelier*
Departamento de Matemática Aplicada-IMECC, Universidade Estadual de Campinas, 13081-970 Campinas, S.P., Brazil

The Rayleigh criterion is used to study the stability of circular orbits of particles moving around static black holes surrounded by different axially symmetric structures with reflection symmetry, like disks, rings and halos. We consider three models of disks one of infinite extension and two finite, and one model of rings. The halos are represented by external quadrupole moments (either oblate or prolate). Internal quadrupole perturbation (oblate and prolate) are also considered. For this class of disks the counter-rotation hypothesis implies that the stability of the disks is equivalent to the stability of test particles. The stability of Newtonian systems is also considered and compared with the equivalent relativistic situation. We find that the general relativistic dynamics favors the formation of rings.

PACS numbers: 04.70.Bw, 95.10.Eg, 98.35.Mp, 98.62.Mw

arXiv:gr-qc/0309033v1 5 Sep 2003

I. INTRODUCTION

One of the main tools used to study the gravitational field of any distribution of mass, e.g., a black hole (BH), is to examine the motion of nearby test particles. In other words, the complete understanding of the different solutions of the geodesic equation leads us to the comprehension of the gravitational properties of the center of attraction, in the present case a black hole surrounded by and axially symmetric structure. Because of its mathematical simplicity and physical relevance circular orbits play a particularly important role in the study of the gravitational properties of a central body. Also circular orbits usually represent limit situations between different regimes.

The purpose of this paper is to study the stability of circular orbits in different gravitating systems formed by a BH surrounded by axially symmetric structures. In particular, we study orbits in BH + disks systems, BH + rings systems, and BH +multipolar fields. In the case of orbits inside the matter, e.g. a disk, we have that in general the stability of the circular orbits can be associated to the stability of the matter itself. The method used to study the stability is the Rayleigh criteria of stability (RCS) for a rotating fluid [1] that can be easily adapted to the study of orbits of test particles. In the context of general relativity the RCS has been used to study the stability of different classes of self-gravitating disks, see for instance [2]-[4].

The paper is divided as follows: In Sec. II we review the RCS and in Sec. III the Einstein equations for the superposition of a static BH and an axially symmetric structure with reflection symmetry is presented. In Sec. IV the stability of circular orbits moving around the superposition of a BH and three models of disks are considered, one of infinite extension and two finite. In Sec. V we study the stability of particles orbiting on the plane of a ring + BH system, inside as well as outside the ring. In Sec. VI we consider circular orbits for a BH perturbed by either an internal quadrupole field or a external quadrupole field. We consider oblate as well as prolate quadruples. We have that some general features found in the study of the previous examples can be simulated with these quadrupole fields. In the last section we discuss some of the previously found results. We also review in an Appendix the so called counter-rotating hypothesis.

II. RAYLEIGH CRITERIA OF STABILITY

Consider, in Newtonian dynamics, a small body of mass μ moving in a circular orbit of radius $r = r_0$ around a fix center of gravitational attraction. In the non inertial frame associated to the moving body we have an equilibrium situation: the gravitational force $[F_g(r_0)]$ is equal to the centrifugal force $[F_c(r_0) = L^2(r_0)/(\mu r_0^3)]$, where L is the angular momentum of the particle of mass μ. Now let us virtually displace the moving particle to a higher orbit ($r > r_0$) keeping the same angular momentum. Then the centrifugal force in this new position is $\hat{F}_c(r) = L^2(r_0)/(\mu r^3)]$. To have a situation of equilibrium the displaced particle should move downward, i.e., in direction to the initial orbit. In other words, the gravitational force in r should be greater than the centrifugal force, $\hat{F}_c(r)$, i.e., $F_g(r) > \hat{F}_c(r)$, but $F_g(r) = F_c(r) = L^2(r)/(\mu r^3)$. Hence $L^2(r) > L^2(r_0)$, by doing a Taylor expansion of $L^2(r)$ around $r = r_0$ we find that, $L\frac{dL}{dr} > 0$, for a stable circular orbit. Rayleigh in the original derivation of his criterion [1], considers a rotating ring of fluid under the force of a pressure gradient instead of a the particle moving in a circular orbit attracted by a gravitational field.

Now let us consider a particle moving in a static background metric with axial symmetry in spherical co-

*e-mail: letelier@ime.unicamp.br

ordinates, $(t, R, \vartheta, \varphi)$,

$$ds^2 = g_{tt}dt^2 + g_{RR}dR^2 + g_{\vartheta\vartheta}d\vartheta^2 + g_{\varphi\varphi}d\varphi^2, \quad (1)$$

where the metric functions $g_{\mu\nu}$ depends only on the variables R, ϑ. The geodesic equation for a circular motion on the plane $\vartheta = \pi/2$, gives us the motion equation,

$$g_{tt,R}\dot{t}^2 + g_{\varphi\varphi,R}\dot{\varphi}^2 = 0, \quad (2)$$

and the constants of motion,

$$1 = g_{tt}\dot{t}^2 + g_{\varphi\varphi}\dot{\varphi}^2, \quad (3)$$
$$E = g_{tt}\dot{t}, \quad (4)$$
$$h = g_{\varphi\varphi}\dot{\varphi}, \quad (5)$$

where the orverdot denotes derivative with respect to the proper time s and $g_{tt,R} = \partial_R g_{tt}$, etc. The constant E represents the relativistic specific energy and h the specific angular momentum.

Note that the motion equation (2) can be cast as a balance equation valid on the plane $\vartheta = \pi/2$,

$$g_{tt,R}E^2/g_{tt}^2 = -g_{\varphi\varphi,R}h^2/g_{\varphi\varphi}^2. \quad (6)$$

So as in the Newtonian case we have a balance between the "gravitational force" and the "centrifugal force". Thus, assuming the metric represents the gravitation of a central body we will have stability of circular orbits on the plane $\vartheta = \pi/2$, when

$$hh_{,R} > 0. \quad (7)$$

From (2)- (5)we find,

$$h^2 = -\frac{g_{\varphi\varphi}^2 g_{tt,R}}{g_{tt}g_{\varphi\varphi,R} - g_{tt,R}g_{\varphi\varphi}}, \quad (8)$$

$$E^2 = \frac{g_{tt}^2 g_{\varphi\varphi,R}}{g_{tt}g_{\varphi\varphi,R} - g_{tt,R}g_{\varphi\varphi}}. \quad (9)$$

Since gravity is an attractive force we can repeat the same reasoning that leads to (7), but now with the constant $E(R, \pi/2)$ instead of $h(R, \pi/2)$, we find

$$EE_{,R} > 0. \quad (10)$$

From (8) and (9) we get,

$$hh_{,R} = -\frac{g_{\varphi\varphi}}{g_{tt}}EE_{,R}. \quad (11)$$

But, always $-g_{\varphi\varphi}/g_{tt} > 0$, then the relation (10) gives us the same information than (7), in other words we have consistence.

For the stability of circular orbits in stationary axisymmetric spacetimes see Ref. [5] and for stability of rotating fluids in a relativistic stars see Ref. [6]. This last reference presents a very general study of the stability of relativistic fluids that generalizes the Lord Rayleigh work by considering a relativistic fluid with both bulk and dynamical viscosity and also heath flow. A slightly different treatment of the stability of circular orbits like the one presented here can be found in Ref. [7].

III. WEYL METRICS: BLACK HOLES + AXIALLY SYMMETRIC STRUCTURES

The external gravitational field produced by an axially symmetric body can be well described by the Weyl metric [8],

$$ds^2 = e^{2\psi}dt^2 - e^{-2\psi}[r^2 d\varphi^2 + e^{2\gamma}(dr^2 + dz^2)], \quad (12)$$

where the functions ψ and γ depend only on the cylindrical coordinates r and z. The vacuum Einstein equations ($R_{\mu\nu} = 0$) reduce to the usual Laplace equation in cylindrical coordinates,

$$\psi_{,rr} + \psi_{,r}/r + \psi_{,zz} = 0, \quad (13)$$

and the quadrature,

$$d\gamma[\psi] = r[(\psi_{,r}^2 - \psi_{,z}^2)dr + 2\psi_{,r}\psi_{,z}dz]. \quad (14)$$

When ψ satisfies the Laplace equation this differential is exact.

The Schwarzschild solution in Weyl coordinates takes the form,

$$\psi_S = \frac{1}{2}\ln\frac{R_+ + R_- - 2m}{R_+ + R_- + 2m}, \quad (15)$$

$$\gamma_S = \frac{1}{2}\ln\frac{(R_+ + R_-)^2 - 4m^2}{R_+ R_-}, \quad (16)$$

where

$$R_\pm = \sqrt{r^2 + (z \pm m)^2}. \quad (17)$$

The function ψ_S is just the Newtonian potential of a bar of length $2m$ and density $1/2$. The Weyl coordinates has the drawback that the Schwarzschild metric does not look spherically symmetric and that the horizon is squeezed into a line of length $2m$. But has the advantage that one of the Einstein equations is the Laplace equation that is linear, hence it allows to consider different composite systems like a black hole surrounded by disks or halos in an exact way.

The coordinate transformations,

$$r = [R(R - 2m))]^{\frac{1}{2}}\sin\vartheta, \quad z = (R - m)\cos\vartheta, \quad (18)$$

takes the black hole metric (12) with (15)-(16) into the usual Schwarzschild form.

We shall consider solutions of the form,

$$\psi = \psi_S + \hat{\psi}, \quad (19)$$

where $\hat{\psi}(r, z)$ is a solution of either Laplace equation or Poisson equation with a density that has support on the plane $z = 0$ ($\vartheta = \pi/2$). The function γ in this case is also written as

$$\gamma[\psi] = \gamma_S + \hat{\gamma}(r, z). \quad (20)$$

In the case of vacuum solutions $\hat{\gamma}(r,z)$ can be computed directly from (14) and (19).

Therefore for the superposition (19) the Weyl metric takes the form,

$$ds^2 = (1-\frac{2m}{R})e^{2\hat{\psi}}dt^2 - \frac{e^{2(\hat{\gamma}-\hat{\psi})}}{1-\frac{2m}{R}}dR^2 - R^2e^{-2\hat{\psi}}(e^{2\hat{\gamma}}d\vartheta^2+\sin^2\vartheta d\varphi^2). \quad (21)$$

When $\hat{\psi}=\hat{\gamma}=0$ we recover the Schwarzschild metric.

We shall analyze three types on superpositions of BH and matter. In the first, the matter is represented by a potential $\hat{\psi}$ that describes a thin disk. In this case we will have that only two components of energy-momentum tensor (EMT), T^t_t and T^φ_φ, are different from zero on the plane of the disk. Thus we have a disk with no radial pressure or tension to support the gravitational attraction. Since the Weyl metric is static we have no rotation. Then a counter-rotation hypothesis is needed to have a stable situation: we assume that on the disk as many particles move clockwise as counterclockwise (see Appendix A). Even though, this interpretation can be seen as a device, there is observational evidence of disks made of streams of rotating and counter-rotating matter [9]. We believe that counter rotating hypothesis appeared first, in this context, in Ref. [10].

In the general case we will have radial pressure and magnetic forces and our simpler analysis need to be modified. In the case when no magnetic fields are present and the density and pressure of the matter of the disk are low, e.g., a diluted gas of stars, the main contribution to the force on each fluid particle is the gravitational force that is taken into account through the spacetime metric.

In the second case we study the superposition of a BH and a thin ring. We consider orbits inside the ring as well as orbits outside the ring. And in the third case we consider the superposition of a BH with multipolar fields. We first consider internal multipolar perturbations, i.e., $\hat{\psi}$ is a multipolar field that is zero at spatial infinite. In this way we can describe the gravity outside compact systems formed by a true black hole (or a dense object) surrounded by a distribution of matter like a ring or a small disk. Also we can have an axially symmetric static dense object with either polar deformations or polar jets. We also consider the case of a BH with external multipolar perturbations, i.e., $\hat{\psi}$ is a multipolar field, solution of Laplace equation (13), that diverges at spatial infinite. In this case we can represent the gravity in the region limited by a black hole and an outer axially symmetric shell of matter or halo.

All the models of BH with surrounded matter that we consider in this paper are constructed from superposition of the Weyl solutions of the form (20) and its associated spacetime is described by the metric (21). In this case the constant of motion (5) takes the form,

$$h^2 = \frac{R^2e^{-2\hat{\psi}}[m+R(R-2m)\hat{\psi}_{,R}]}{R-3m-2(R-2m)\hat{\psi}_{,R}}, \quad (22)$$

and its derivative can be cast us,

$$hh_{,R} = \frac{Re^{-2\hat{\psi}}[m(R-6m)+F_1]}{2(R-3m-2F_2)}, \quad (23)$$

where

$$\begin{aligned} F_1 &= R(28m^2-18mR+3R^2)\hat{\psi}_{,R} - \\ &\quad 6R^2(R-3m)(R-2m)\hat{\psi}^2_{,R}+4R^3(R-2m)^2\hat{\psi}^3_{,R} \\ &\quad +R^2(R-m)(R-2m)\hat{\psi}_{,RR}, \quad (24) \\ F_2 &= R(R-2m)\hat{\psi}_{,R} \quad (25) \end{aligned}$$

In the present case the motion is limited to the plane $z=0(\vartheta=\pi/2)$. From (18) we have that $r=[R(R-2m))]^{\frac{1}{2}}$ on the plane and $\hat{\psi}(r,0)=\hat{\psi}([R(R-2m))]^{\frac{1}{2}},0)$. Note that when $\hat{\psi}=0$, pure BH case, from (23) and $hh_{,R}=0$ we have $R=6m$, as required. This orbit is known as the last stable circular orbit (LSCO) or the marginally stable circular orbit (MSCO). In our study of stability we will use Schwarzschild like coordinates. The use of Weyl coordinates or proper distance coordinates are known to give similar qualitative results [11].

IV. BH + DISKS

In this section we study the superposition of a BH and three different models of disks. In the first case the disk is the relativistic generalization of the Newtonian Kuzmin disk that is studied in Ref. [2]. This solution is closely related to the vacuum solution of the Einstein equation known as Chazy-Curzon metric [12]. The metric function $\hat{\psi}$ for the superposition of this disk with a BH is,

$$\hat{\psi}(r,0) = -M/(r^2+a^2)^{\frac{1}{2}} \quad (26)$$

The disk has mass M an infinite radius, a is a parameter related to the maximum of the energy density.

The second and third model of disks are the zeroth and first Morgan and Morgan disks [10] that are obtained by solving the Laplace equations in oblate coordinates. The function $\hat{\psi}(r,0)$ for the zeroth order Morgan and Morgan disk is

$$\hat{\psi}(r,0) = -\frac{M}{a}\arctan\frac{a}{\sqrt{r^2-a^2}}, \quad r>a \quad (27)$$

$$\hat{\psi}(r,0) = -\frac{\pi M}{2a}, \quad r<a. \quad (28)$$

M represents the mass of the disk and a its radius. This disk has infinite density on the edge. The superposition of this disk and a BH is studied in [13].

For the first Morgan and Morgan disk we have,

$$\hat{\psi} = -\frac{3M}{4a^2}[\sqrt{r^2-a^2}-a^{-1}(r^2-2a^2)\arctan\frac{a}{\sqrt{r^2-a^2}}, \quad r>a. \quad (29)$$

$$\hat{\psi} = -\frac{3\pi M}{4a^3}(a^2-r^2/2), \quad r<a \quad (30)$$

Again M is the mass of the disk and a its radius. The superposition of this disk with a BH was studied in [14][15]. This disk has finite density on the rim. For simplicity we have presented the potentials Weyl coordinates (t, r, z, φ). We note that to a disk of radius a in Weyl coordinates corresponds a disk of radius

$$R_a = m + \sqrt{m^2 + a^2}, \tag{31}$$

in the usual BH coordinates that will be used in our analysis of stability. We shall study numerically the condition $hh_{,R} = 0$ that will give us information on the stability of circular orbits for the different superpositions of BH and disks.

For the Kuzmin-Chazy-Curzon disk in Fig 1 we study the curve $hh_{,R} = 0$ for different values of the parameter a, we take $a = 0.5, 2.5, 4.5, 6$. Along all this work we take units such that $G = c = 1$ and we fix the unit of length by taking the mass of the central BH as one. We have stability in the regions limited by the upper curves and the axis R and in regions limited by the lower curves and $R = 2m$. In the first case, $a = 0.5$, for a given total mass parameter of the disk, M, we have a region, close to the BH horizon, wherein we have stable circular orbits. For larger values of R we have a region of instability. In principle this region of instability will give rise to a gap in the disk. For even larger values of R we will have another region of stability that extent to infinite. In the second case, $a = 2.5$, closer to the horizon, for $4 < M < 6$, will appear another region of instability. So we can have the formation of stable flat rings in this region. In the third case, $a = 4.5$ we can have rings around $M = 3$ and for $M > 8$. In the last case, $a = 6$, rings can also be formed. It is interesting to compare this case with the equivalent Newtonian situation. By applying the RCS to the system represented by the Newtonian potential

$$\phi = -M/(R^2 + a^2)^{\frac{1}{2}} - m/R \tag{32}$$

we find only stable circular orbits. Therefore the formations of rings and gaps, in the present case, is a pure general relativistic effect.

Now we shall consider the zeroth order Morgan and Morgan disk. In the interior of the disk we have that the function $\hat{\psi}$ is constant. Hence the condition $hh_{,R} = 0$ gives us $R = 6m$, the LSCO of the usual BH. Therefore if the radius of the disk is less than $6m$ it is completely unstable. For a disk of radius grater than $6m$ we will have that the region of the disk between $6m$ and its radius will be stable. The condition $hh_{,R} = 0$ outside the disk is studied in Fig 2.

We have stability in the region limited by the upper curve and the axis R and in the region limited by the lower curve and the horizontal line that represents the radius of the disk. Therefore we can have the formation of a stable structure orbiting around the disk close to its edge. After this zone of stability we find a zone of instability followed by one of stability.

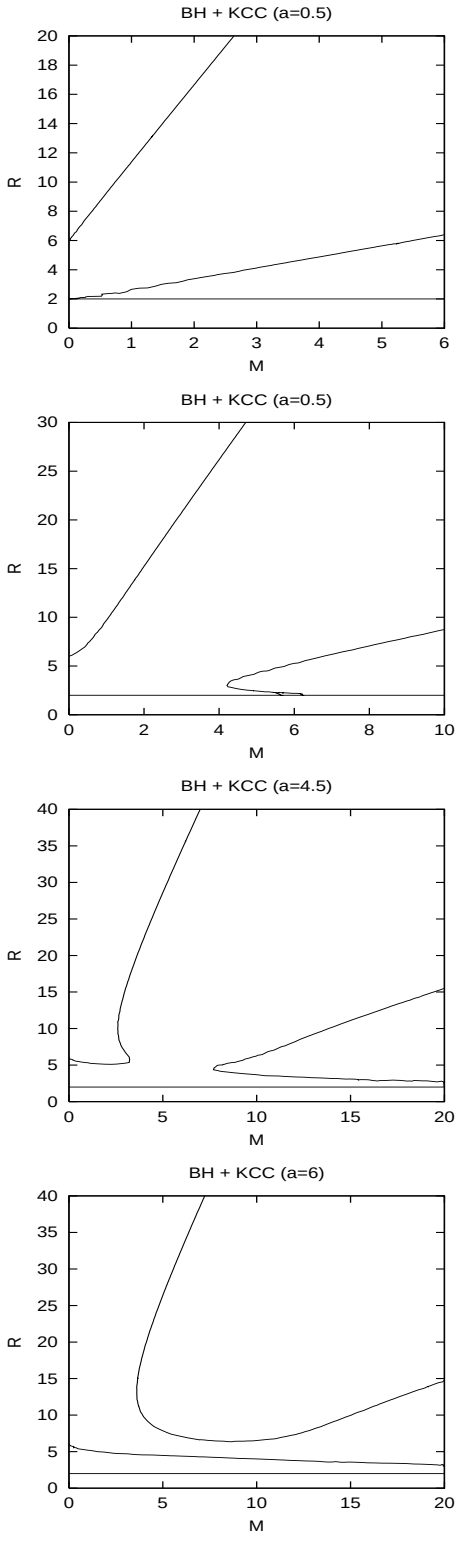

FIG. 1: Curves $hh_{,R} = 0$ for the superposition of a BH and a Kuzmin-Chazy-Curzon disk for different values of the parameter a. The curve, $R = 2m$, is also shown. In the first three cases we have stability in the regions limited by the upper curves and the axis R and in the regions limited by the lower curves and $R = 2m$. In the last case we have stability in the region limited by the upper curve and the lower curve. We use units such that $G = c = m = 1$.

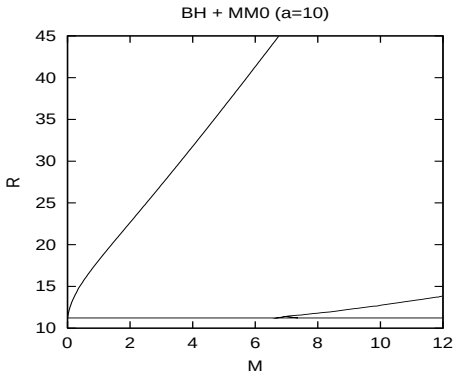

FIG. 2: Curves $hh_{,R} = 0$ for the superposition of a BH and a zeroth order Morgan and Morgan disk for $a = 10$. The horizontal line indicates the position of the disk boundary. We have orbit stability in the region limited by the upper curve and the axis R and in the region limited by the lower curve and radius of the disk. The units are the same as in the previous figure.

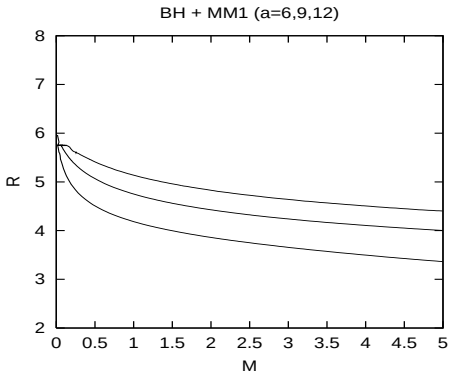

FIG. 3: Curves $hh_{,R} = 0$ for the superposition of a BH and the first Morgan and Morgan disk. The top curve represent a disk with parameter $a = 12$, the middle with $a = 9$ and the bottom curve with $a = 6$ We have stable circular orbits in the region above each respective curve.

It is instructive to compare these results with the equivalent Newtonian situation that is represented by the potential,

$$\phi = -\frac{M}{a}\arctan\frac{a}{\sqrt{R^2 - a^2}} - \frac{m}{R}. \tag{33}$$

We find a very different situation, we only have a small zone of instability close to the disk boundary. The interior of the disk is stable.

Now we shall consider the superposition of first Morgan and Morgan disk with a BH. In Fig 3 we present the curve $hh_{,R} = 0$ for three different disks with parameters $a = 12$ (top curve), $a = 9$, and $a = 6$ (bottom curve). We have a region of instability in the region under the curve $hh_{,R} = 0$ in each case. We have that the presence of a disk lower the black hole's LSCO.

The curves $hh_{,R} = 0$ for the superposition of a BH and the first Morgan and Morgan disk with $a = 9$ is presented in Fig. 4 for a region outside the disk. We have that the closer to the edge of the disk we always have unstable circular orbits. For larger radius we have stable orbits.

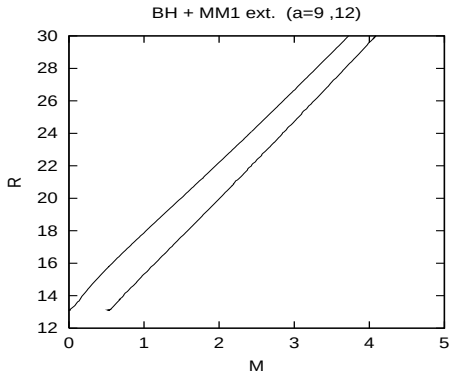

FIG. 4: Curves $hh_{,R} = 0$ for the superposition of a BH and the first Morgan and Morgan disk with $a = 9$ (bottom curve) and $a = 12$ (top curve). We have stable circular orbits in the region limited by the curve and the axis R.

It is interesting to compare this case with the same Newtonian situation. For the interior of the disk with a Newtonian center of attraction we find no regions of instability. Outside the disk the situation is similar to the one shown in Fig. 4, but in the Newtonian case the curves are lower.

The superposition of the BH with the zeroth order Morgan and Morgan disk and with the first Morgan and Morgan disk present different properties of stability near the edge of the disk. We have that the first mentioned disk has a singular rim and the second has a regular edge. This last case represent a physically acceptable situation.

V. BH + RINGS

In this section we consider the superposition of a black hole and a family of thin rings. The function $\hat{\psi}$ for the thin rings will be taken as,

$$\hat{\psi} = -\frac{M}{2}[\frac{1}{\sqrt{r^2 - r^2}} + \arctan\frac{a}{\sqrt{r^2 - a^2}}],\ r > a \tag{34}$$

$$\hat{\psi} = -\frac{M}{2}[\frac{1}{\sqrt{a^2 - r^2}} + \frac{\pi}{2}], \quad r < a. \tag{35}$$

The parameters M and a represent the mass and radius of the ring, respectively. This family of thin rings as well as its superposition with a black hole is studied in some detail in [13].

In Fig. 5 we consider the curve $hh_{,R} = 0$ for the superposition of a BH and the ring with potential $\hat{\phi}$ given by (34)-(35). The first graph shows the region exterior to the ring and the second the interior region for $a = 8$ (left hand side curve) and $a = 10$ (right hand side curve). For $a = 8(a = 10)$ we have $R_8 \sim 9(R_{10} \sim 11)$.

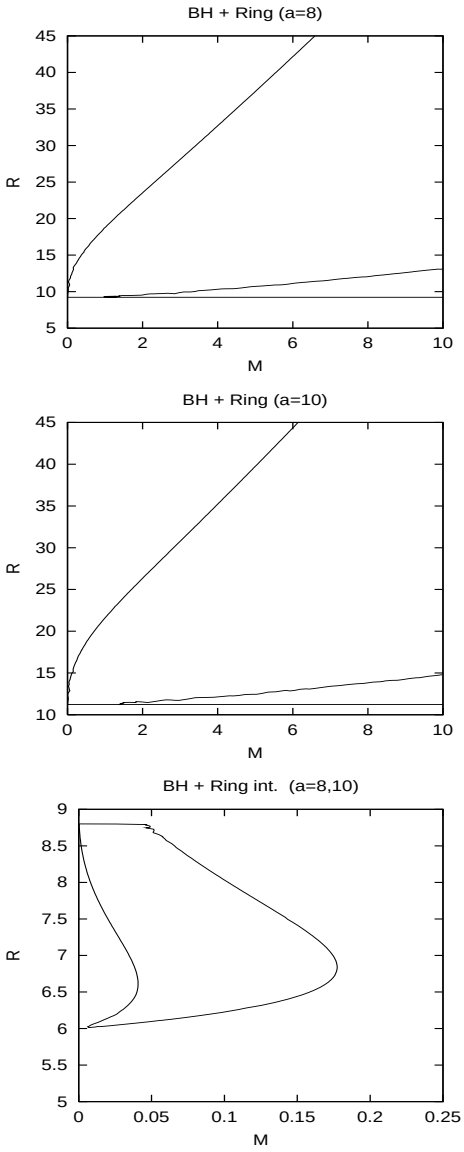

FIG. 5: Curves $hh_{,R} = 0$ for the superposition of a BH and a thin ring. The first two graphs show the region exterior to rings with $a = 8$ and $a = 10$ and the third the interior region for rings of the same radii the LHS (RHS) curve correspond to $a = 8(10)$. In the first two graphs we have stable circular orbits in the the regions limited by the upper curves and the axis R and in the regions limited by the lower curves and the horizontal line that represents the location of the ring. In the third graph we have stable circular orbits in the region limited by the corresponding curve and the axis R.

For the exterior region we have stable circular orbits for values of (M, R) limited by the upper curve and the axis R and in the region limited by the lower curves and the horizontal line that represents the location of the ring. In the third graph we have stable circular orbits in the region limited by the corresponding curve and the axis R.

The regions of stability for the equivalent Newtonian situation are different. We have only one small region of instability of circular orbits with radii larger to the ring radius. For the interior of the ring we have that the curve $hh_{,R} = 0$ is similar to the precedent case for values of R close to the ring radius. The Newtonian case is similar to the relativistic case, but the curve does not turns back to $R = 6m$ it decreases as $R \sim 1/M^{1/3}$. The analysis of stability of circular orbits for the superposition of a BH and a flat ring (Lemos-Letelier solution [14]), as well as other aspects of this solution were considered in great detail in [16], [11], and [17].

VI. BH + MULIPOLAR FIELDS

Multipolar exact perturbation of a BH can approximate all situations studied in the previous sections of this article that refer to compact sources of gravity. Also we can have some insight for the stability of circular orbits in the generic case of a static BH with axially symmetric perturbations with reflection symmetry.

The functions $\hat{\psi}(r, z)$ in the present case are

$$\hat{\psi}(r, 0) = -Q_i/r^3 \tag{36}$$

$$\hat{\psi}(r, 0) = -Q_e r^2 \tag{37}$$

Where Q_i represents the quadrupolar moment of an internal distribution of matter, i.e., of sources of the gravitational field near the BH, e.g., disks, rings, etc. This field will approximate the gravitation field outside its source. We have two cases $Q_i > 0$ and $Q_i < 0$. The first case represents oblate deformations like disks and rings and the second prolate deformations, e.g., jets. The constant Q_e is related to the quadrupolar moment of external distributions of matter, i.e., of sources of the gravitational field far away from the BH, e.g, the gravity in the space limited by a ring or a shell of matter (halo). We also have two different situations in this case $Q_e > 0$ and $Q_e < 0$. The first case describes oblate deformations like a ring or oblate halos and the second prolate deformations like prolate halos.

In Fig. 6 we present curves $hh_{,R} = 0$ for the superposition of a BH and an internal multipolar field with $\hat{\phi}$ give by (36). The first graph shows the oblate case and the second prolate deformations. In the oblate case we have stable circular orbits in the the regions limited by the upper curve and the axis R and in the regions limited by the lower curves and the horizontal line that represents the BH horizon. The most relevant region is the one with $R > 6m$. We see that the region of stability increases with the internal quadrupole moment. It is interesting to compare this result with the previous case. Let us consider the superposition of a BH with the first Morgan and Morgan disk. We see in Fig 4 that for a given disk mass the region of instability increases with the disk radius the same is true for rings, see Fig 5. We also checked this property for the zeroth order Morgan and Morgan disk. We have, for these compact

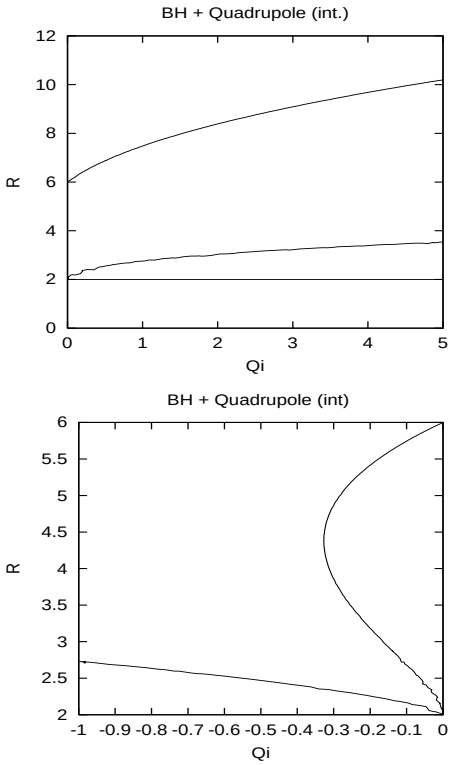

FIG. 6: Curves $hh_{,R} = 0$ for the superposition of a BH and an internal quadrupolar field. The first graph shows the oblate case and the second the prolate deformations. In the first we have stable circular orbits in the the regions limited by the upper curve and the axis R and in the regions limited by the lower curves and the horizontal line that represents the BH horizon. In the second graph we have stable circular orbits in the region limited by the axis R and the curves.

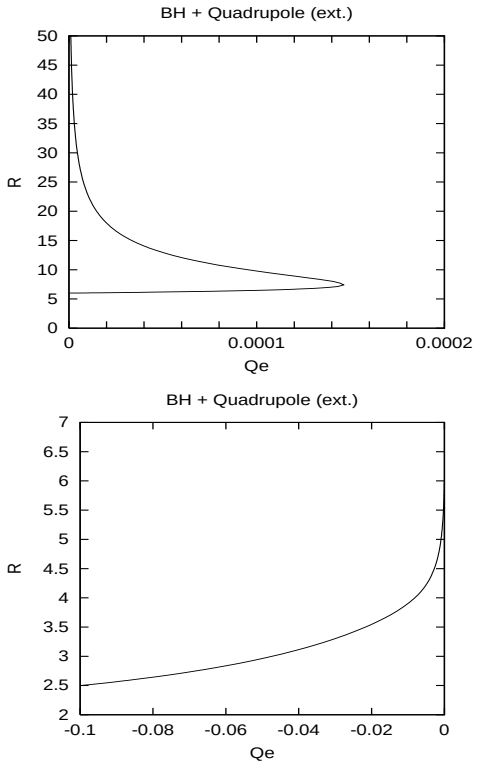

FIG. 7: Curves $hh_{,R} = 0$ for the superposition of a BH and an external quadrupolar field. In the first graph , oblate case, we have stable circular orbits in the the regions limited by the curve and the axis R. In the second graph, prolate case, we have stable circular orbits in the region above the curve.

objects, that the quadrupolar moments scale as $Q_i \sim Ma^2$. Therefore to a bigger radius corresponds a bigger quadrupole moment and a larger region of instability.

In the prolate case, last graph of Fig. 6 we see that the quadrupole moment increases the zone of stability, with no quadrupole moment we have stability only when $R > 6m$. This is a rather surprising effect valid only for equatorial circular orbits. For generic orbits, a prolate internal deformation introduces great instability, moreover we can have very irregular orbits (chaos) [18].

In the equivalent Newtonian system, for the oblate case we have a region of instability near the center of attraction. The limit curve is $R = (\sqrt{3Q_i/m}$. We have no instability in the prolate case. Again for non equatorial circular orbits we can have chaotic motion in this case [18].

In Fig. 7 we present curves $hh_{,R} = 0$ for the superposition of a BH and external multipolar field with $\hat{\phi}$ give by (37). In the first graph, oblate case, we have stable circular orbits in the the regions limited by the curve and the axis R. We have that this external quadrupole fields severely restrict the possibility of stable orbits. We have that for larger value of $Q_e > 0.00015$ we do not have equatorial stable circular orbits. For $Q_e < 0.00015$ we have that the region of stability is limited from above as well as from below. For generic orbits in BH exterior halo systems we have chaotic orbits [19].

We have that the exterior quadrupole moment of a ring or any external configuration of matter like a shell or halo scales as $Q_e = M/a^3$, with M the mass of the shell and a the typical size. Then large radius indicates small quadrupole moment and large stability region. We note that second graph of Fig. 5 illustrate exactly this conclusion. In the equivalent Newtonian case we have that the curve $hh_{,R} = 0$ is $R = (m/8Q_e)^{1/3}$.

In the prolate case, second graph of Fig. 7, we have stable circular orbits in the region above the curve. We see that the prolate external matter increases the region of stability. For the Newtonian equivalent system we always have stable orbits. Marginally stable orbits in quadrupole deformed centers of attraction were also studied in [20].

VII. CONCLUDING REMARKS

We think that one of the most important results shown in this paper is that we can have the formations of rings and gaps around a BH as a pure general relativistic

effect, of course this is a consequence of the presence of the BH horizon that modifies the usual Newtonian effective potential adding new critical points. These critical points change completely the dynamics of the orbiting particles. In particular, the maximum has the property of being a saddle point in phase space. Hence perturbed orbits tend to have irregular motions.

The use of multipoles to represent a distribution of matter in the general relativistic context need to be taken with care. In general relativity, the multipolar expansion take into account that we have a tensorial source of the gravitational field and not a scalar one as in Newtonian gravity. We can have different sets of general relativistic multipoles that in the limit of Newtonian gravity give the same set of usual Newtonian multipoles, for a discussion of this point in the context of static axially symmetric spacetimes see [21]. We found for orbits that are a few Schwarzschild radius away from the center of attraction no significant discrepancy due the use of different multipolar expansion with the same Newtonian limit [21]. Hence there is no great error in taken any multipolar expansion with the same Newtonian limit, the one taken in this paper is the simpler.

Our study of chaos in BH with halos [19] and deformed centers of attractions [18] indicates that the stability of circular orbits is quite different from the stability of generic orbits. This is not a surprising result since the equatorial circular orbits are a very special case of highly symmetric orbits.

Acknowledgments

I want to thank FAPESP and CNPQ for financial support and Prof. Opher for getting me interested in the subject of this paper.

APPENDIX A: THE COUNTER-ROTATING HYPOTHESIS

The EMT for the counter-rotating matter is the sum of the energy momentum tensor of two pressureless streams of particles,

$$T^{\mu\nu} = T^{\mu\nu}_+ + T^{\mu\nu}_- \tag{A1}$$

where

$$T^{\mu\nu}_+ = \rho_+ U^\mu_+ U^\nu_+, \;\; T^{\mu\nu}_- = \rho_- U^\mu_- U^\nu_-. \tag{A2}$$

ρ_+ and ρ_- are the matter density of each stream that are considered equal ($\rho_+ = \rho_-$). U^μ_+ and U^μ_- are the corresponding normalized streams' four-velocities ($U^\mu_+ U_{+\mu} = U^\mu_- U_{-\mu} = 1$). These four velocities can be written as

$$U^\mu_+ = \alpha U^\mu + \beta\phi^\nu, \;\; U^\mu_- = \alpha U^\mu - \beta\phi^\nu, \tag{A3}$$

where U^μ is a timelike vector and ϕ^ν an spacelike vector tangent to one of the two streams of particles, also $U^\mu U_\mu = -\phi^\nu\phi_\nu = 1$, $U^\mu\phi_\nu = 0$. Note that $\alpha^2 - \beta^2 = 1$. Therefore the EMT (A1) can we put in the form

$$T^{\mu\nu} = \rho U^\mu U^\nu + p_\phi \phi^\mu \phi^\nu, \tag{A4}$$

with $\rho = 2\alpha^2\rho_+$ and $p_\phi = 2(1-\alpha^2)\rho$.

Thus the counter-rotating hypothesis is consistent with the disks represented by the Weyl metrics solutions to the Einstein equations that have only azimuthal pressure. Furthermore we can assume that

$$\nabla_\mu T^{\mu\nu}_+ = \nabla_\mu T^{\mu\nu}_- = 0. \tag{A5}$$

From (A2) we have $U^\mu_+ \nabla_\mu U^\nu_+ = U^\mu_- \nabla_\mu U^\nu_- = 0$, i.e., each stream follows a geodesic motion. Note that (A5) implies that $\nabla_\mu T^{\mu\nu} = 0$. Thus the supposition that each stream follows a geodesic flow is consistent with the Bianchi identity for the Weyl metric. For multifluids, see for instance Ref. [22].

In summary, when the counter-rotating hypothesis is assumed, the stability of circular geodesics is equivalent to the stability of the flow of each fluid component. For the counter-rotating model of cold disks we have that the LSCO defines exactly the inner radius of the disk.

[1] Lord Rayleigh, Proc. R. Soc. Lond. Ser. A 93, 148 (1916). See also, L. D. Landau, E. M. Lifshitz, "Fluid Mechanics", 2nd Ed. (Pergamon Press, Oxford, 1987), §27.
[2] J. Bičák, D. Lynden-Bell and J. Katz, Phys. Rev. D47, 4334 (1993)
[3] P. S. Letelier. Phys. Rev. D 60, 104042-1 (1999).
[4] D. Vogt and P.S. Letelier, Phys. Rev. D, to appear. Available at http://xxx.lanl.gov/abs/gr-qc/0308031.
[5] J.M. Bardeen, Ap. J., 161, 103 (1970).
[6] F.H. Seguin, Ap. J. 197, 745 (1975).
[7] M.A. Abramowicz, Mon. Not. R. astr. Soc. 245, 720 (1990).
[8] See for instance, H. Robertson and T. Noonan, "Relativity and Cosmology"(Saunders, London 1968) pp 272-278.
[9] F. Bertola *et al.* Ap. J. 458, L67 (1996).
[10] T. Morgan and L. Morgan, Phys. Rev. 183, 1097 (1969).
[11] O. Semerák and M. Žáček, Publ. Astron. Soc. Japan, 52, 1067 (2000)
[12] M. Chazy, Bull. Soc. Math. France 52, 17 (1924); H. Curzon, Proc. London Math. Soc. 23, 477 (1924).
[13] P.S. Letelier and S.R. Oliveira , Class. Quantum Grav. 15, 421 (1998)
[14] J.P.S. Lemos and P.S. Letelier, Phys. Rev. D 49, 5135 (1994).

[15] J.P. Lemos and P.S. Letelier, Class. Quantum Grav. 10, L75 (1993)
[16] O. Semerák and M. Žáček, Class. Quantum Grav. 17, 1613 (2000).
[17] O. Semerák, Class. Quantum Grav. 20, 1613 (2003).
[18] E. Guéron and P.S. Letelier, Phys. Rev. E 66, 046611 (2002); *ibid* 63, 035201(R), (2001).
[19] W.M. Vieira and P.S. Letelier, Ap. J. 513, 383 (1999).
[20] J.L. Zdunik and E. Gourgoulhon, Phys. Rev. D 63, 087501 (2001).
[21] B. Boisseau and P.S. Letelier, Gen. Rel. Grav. 34, 1077 (2002)
[22] P.S. Letelier, Phys. Rev. D 22, 807 (1980)